Self-floating carbon nanotube membrane on macroporous silica substrate for highly efficient solar-driven interfacial water evaporation

Article

Self-floating carbon nanotube membrane on macroporous silica substrate for highly efficient solar-driven interfacial water evaporation

Yuchao Wang, Lianbin Zhang, and Peng Wang

ACS Sustainable Chem. Eng., **Just Accepted Manuscript** • DOI: 10.1021/acssuschemeng.5b01274 • Publication Date (Web): 22 Jan 2016

Self-floating carbon nanotube membrane on macroporous silica substrate for highly efficient solar-driven interfacial water evaporation

*Yuchao Wang, Lianbin Zhang, and Peng Wang**

Water Desalination and Reuse Center, Division of Biological and Environmental Science and Engineering, King Abdullah University of Science and Technology, Thuwal 23955-6900, Saudi Arabia.

*Corresponding author: Peng Wang, e-mail: peng.wang@kaust.edu.sa.

KEYWORDS: Solar evaporation, photothermal, carbon nanotube, interfacial heating, heat barrier.

ABSTRACT

Given the emerging energy and water challenges facing the mankind, solar-driven water evaporation has been gaining renewed research attention from both academia and industry as an energy efficient means of wastewater treatment and clean water production. In this project, a bi-layered material, consisting of a top self-floating hydrophobic CNT membrane and a bottom hydrophilic macroporous silica substrate, was rationally designed and fabricated for highly energy-efficient solar driven water evaporation based on the concept of interfacial heating. The top thin CNT membrane with excellent light adsorption capability, acted as photothermal

component, which harvested and converted almost the entire incident light to heat for exclusively heating of interfacial water. On the other hand, the macroporous silica substrate provided multi-functions toward further improvement of operation stability and water evaporation performance of the material, including water pumping, mechanical support and heat barriers. The silica substrate was conducive in forming the rough surface structures of the CNT top layers during vacuum filtration and thus indirectly contributed to high light adsorption by the top CNT layers. With optimized thicknesses of the CNT top layer and silica substrate, a solar thermal conversion efficiency of 82 % was achieved in this study. The bi-layered material also showed great performance toward water evaporation from seawater and contaminated water, realizing the separation of water from pollutants, and indicating its application versatility

INTRODUCTION

Solar energy is the ultimate energy source of everything we have on the earth and is without any doubt the most renewable and sustainable energy source available to us. One simple fact is that the solar energy that strikes the earth in a single day is more than the total energy consumption of the entire world in a year. (1-2) Solar-driven water evaporation provides 90 % of moisture in the atmosphere and thus plays a critical role in the global water cycle. Over the history of mankind, this nature's way of solar evaporation has being directly and partially imitated in various forms for beneficial purposes. As a sustainable approach for fresh water production and wastewater treatment, solar-driven water evaporation has long been used in the field of solar still by mariners and industry.(3-4) However, the natural solar driven-water evaporation suffers low energy efficiency majorly due to the fact that water in this system is the substance that adsorbs and converts light to heat. Water is known to be a very poor light absorber in the solar spectrum range and is mainly responsive in the near-infrared light part. As a consequence, incident light

lessens slightly downward through water body and thus travels a great distance before being completely diminished. Generally, there is still 16 % of the incident light energy remaining at the 10-meter depth in clean seawater. This leads to an undesirably uniform temperature profile throughout the light travel path in the water column and thus gives rise to a bulk water heat behavior in the natural solar-driven water evaporation and its human imitated variants.(5) Water evaporation is indeed a surface process, in which only the water molecules located in a very thin surface layer have the opportunity to transport from liquid phase to vapor phase. The bulk water heating involves unnecessarily heating up a significant amount of non-evaporative water in the bulk water region, leading to a high extent of energy waste. Based on the above discussions, an ideal solar-driven water evaporation scheme should simultaneously fulfill the following requirements: (a) the ability to exclusively capture or concentrate wide spectrum of solar light selectively only at the water-air interface, (b) highly efficient conversion of the captured solar energy to heat, and (c) high concentration of the generated heat at the interfacial water, which necessitates a mechanism to minimize heat transfer from the interfacial region to non-evaporative portion of the underlying bulk water.(6) A water heating scheme with these characteristics can be described as an interfacial heating, in contrast to conventional bulk heating.

Based on the interfacial heating concept, a rational design (7) of a highly efficient solar-driven water evaporation system should integrate into one system the following components: (a) it contains a thin but effective photothermal top layer with high absorbance in the wide solar spectrum, leaving minimal light passing through the top layer.(5) Hydrophobicity-induced self-floating capability of the top photothermal layer has been proven beneficial for automated targeting of the interfacial water. (b) The photothermal top layer efficiently converts the light

energy to heat with minimal energy loss via photoluminescence or due to photoelectric and photomagnetic effects. (c) There exists a thermal barrier layer underneath the top photothermal layer to minimize the heat transfer from the interfacial water to the underlying bulk water to further confine the heat only at the interfacial region. The thermal barrier, however, should not block water passage and should be conducive to the upward water transport from the bulk phase for the purpose of continuous water supply to the top interfacial heating layer. It is often too difficult to include all of these functions in one single-component material and thus making a multi-layered material by multiple materials is nowadays a more practical solution as demonstrated in some recent works.(8-9) For example, Chen and co-workers used exfoliated graphite as top photothermal layer and carbon foam as heat barrier.(9) Song and Deng employed gold nanoparticles as photothermal material and air-laid paper as water pump due to its hydrophilic property and heat barrier.(10) In addition, Chen et al. used a monolithic nitrogen-doped macroporous graphene as photothermal material as well as heat barrier and water pump, and achieved a high solar-driven water evaporation performance.(11)

As far as photothermal materials are concerned, gold nanoparticle,(6, 12) carbon dots,(13-14) carbon black,(15) polypyrrol,(5) graphite,(9) and graphene(11) have recently been investigated in the literature. Carbon nanotube (CNT), a material known to be super-black with extremely high absorbance in the entire solar spectrum, has somehow skipped research attention in solar water evaporation field.(16) A recent study reported that a vertically aligned CNT array could adsorb 99.97 % of incident solar light, making it the darkest material in the world.(16-17) Furthermore, similar to other carbon-based materials, CNT converts absorbed light into heat with high efficiency, which makes it an outstanding candidate for photothermal application.(18-20) Other attractive properties of CNTs with respect to application to solar water evaporation

include: their physical, chemical and thermal stability, the ease with which CNTs can be fabricated into thin and porous film or membranes with controlled thickness and pore sizes by simple filtration, spraying coating, spin coating, etc.,(21-23) and their relatively low specific heat capacity (0.50-0.75 J g^{-1} K^{-1}). Technically, the heat capacity of a photothermal material does not affect water evaporation at equilibrium, but it certainly shortens equilibration time and thus accelerates heating process (11, 24-26)

Herein, we designed and fabricated a bi-layered structure by directly coating a multi-walled CNT membrane on top of a macroporous silica material *via* vacuum filtration. The hydrophilic macroporous silica with low thermal conductivity served triple functions: (a) a water pump that continuously pumps water through its interconnected macro-sized channels to the top heating layer *via* capillary action, (b) a heat transfer barrier that reduces the generated heat from being transferred into the underneath bulk water,(11) and (c) a mechanical support that supports the top thin CNT photothermal layer and at the same time makes possible a seamless connection between two distinctive layers. On the other hand, the thin CNT membrane acted as photothermal top layer, which effectively captured almost the entire solar spectrum, and subsequently converted the light to heat with high efficiency. The heat was utilized to generate water vapor from the interfacial region. The bi-layered composite material self-floated on top of water, thanks to the intrinsic hydrophobic nature of the CNT membrane. A water evaporation rate as high as 1.32 kg m^{-2} h^{-1} with solar thermal conversion efficiency at 82% was achieved with an optimized thickness of both CNT top layer and macroporous silica support. Based on the concept of “design-for-purpose”, this rationally designed material exhibited very satisfactory performance in solar water evaporation of clean water, seawater, and contaminated water as well. With the assistance of such bi-layered materials, there is high possibility to realize the fresh

water production in sustainable field using the solar energy. We further believe the results of this work would shed light on wide applications of photothermal-based water evaporation and water distillation.

EXPERIMENTAL SECTION

Chemicals and materials. Tetramethyl orthosilicate (TMOS), hydrochloric acid, acetic acid, nitric acid, ammonium hydroxide aqueous solution, sodium chloride, anhydrous ethanol, sodium dodecylbenzenesulfonate (SDBS), brilliant blue R (BBR), methyl orange (MO), multi-walled carbon nanotube (product number: 724769) were purchased from Sigma-Aldrich. Polyethylene glycol (PEG) with a molecular weight of 10,000 was from Alfa Aesar. All chemicals were used as received. De-ionized water purified in a Milli-Q system was used in all experiments.

Synthesis of macroporous silica substrate. First, 1.2 g of PEG was mixed with 10.0 mL of 10 mmol L^{-1} acetic acid to get a homogeneous solution. Under vigorous stirring at 0 °C, added into the PEG solution was 4.0 g of TMOS for initiatory hydrolysis. After 30 min, a suitable amount of semi-transparent sol (1.0 - 30.0 mL), depending on the targeted thickness of the final silica substrate, was transferred into a polystyrene petri dish with a diameter of 54 mm, which was then sealed off for gelation at 40 °C for 24 h. The gels were then immersed in 50 mL of 1.0 mol L^{-1} ammonium hydroxide solution at 60 °C for another 24 h. Subsequently, the wet silica gel was washed by 0.05 mol L^{-1} nitric acid before drying at 40 °C. A macroporous silica substrate was finally obtained by calcination the gel in air at 650 °C for 5 h with a temperature ramp at 5 °C min^{-1}. The porosity of the resulted CNT layer was calculated by the equation (1) below:

$$\text{Porosity (\%)} = \frac{V_{pore}}{V} \times 100\ \% = \frac{V - m/\rho_{CNT}}{V} \times 100\ \%$$

where m is the mass of CNT layer obtained from the mass difference before and after CNT coating onto the silica support, V is the volume of CNT layer, V_{pore} is the volume of pores inside CNT layer, and ρ_{CNT} is the inherent density of CNT, which is 2.1 g cm^{-3}.

Fabrication of CNT-silica bi-layered material. An aliquot of 2.0 mg of CNTs and 10.0 mg of SDBS were mixed together and uniformly dispersed into 10.0 mL of DI water with the help of a tip ultrasonication device for 2 hours (Sonics & Materials, Inc., GEX 750). Under vacuum filtration, a certain amount of the CNT solution was slowly dropped onto the upper surface of the macroporous silica substrate, which served as the filtration membrane. The bi-layered CNT and silica structure was then washed thoroughly with ethanol and 1.0 M nitric acid solution alternately for several times to remove the surfactant, SDBS. For the purpose of comparison, a self-supporting CNT membrane was similarly prepared by dropping 0.9 mL of 5 mg mL^{-1} CNT solution onto a silicon wafer with an area of 9.0 cm^2, which was then heated at 95 °C for 1 h. All samples were washed thoroughly with ethanol and 1.0 M nitric acid solution alternately for several times to remove the SDBS.

Characterization. Scanning electron microscopy (SEM) images were taken with an FEI Quanta 600 s. TEM images were taken on a FEI-Tecnai T12 microscope operated at 120 kV. The macropore size distribution of the silica support was determined by mercury porosimetry (AutoPore IV 9510, Micromeritics). The diffuse reflectance UV-Vis absorption spectra were recorded on a spectrophotometer (Shimadazu, UV 2550). Contact angles were measured on a commercial contact angle system (OCA 35 of Data-Physics) at ambient temperature using a 3 μL droplet as indicator. FTIR spectra were collected on a Nicolet iS10 FTIR spectrometer. The temperature and the thermal images were captured using a FLIR A655 infrared camera.

Solar evaporation performance measurement. Clean water, seawater, or dye contaminated water was placed in a cylindrical polypropylene (PP) container with a mouth diameter of 3.2 cm. PP cup was used to minimize heat exchange with ambient air due to its low thermal conductivity (~0.2 W m^{-1} K^{-1}). The simulated solar irradiation was provided by a 150 W Oriel Solar Simulator and the light intensity was adjusted to 1,000 W m^{-2}. The prepared bi-layered material with a diameter of 2.5 cm was placed on top of the water in the PP container and the simulated solar light was shined onto the material vertically from the top with a distance of 17 cm. The PP container was placed on an electronic analytical scale which was connected to a computer for real time monitoring of water loss due to evaporation. The water evaporation rate (v) was calculated as below (2):

$$v = \frac{dm}{S \times dt} \quad (2)$$

where m is the mass of evaporated water, S is the surface area of photothermal material, and t is time. It should be pointed out that in calculating the water evaporation rate by the bi-layered material, the mass of water evaporated due to light illumination from the water surface uncovered by the bi-layer material was deducted.

RESULTS AND DISCUSSION

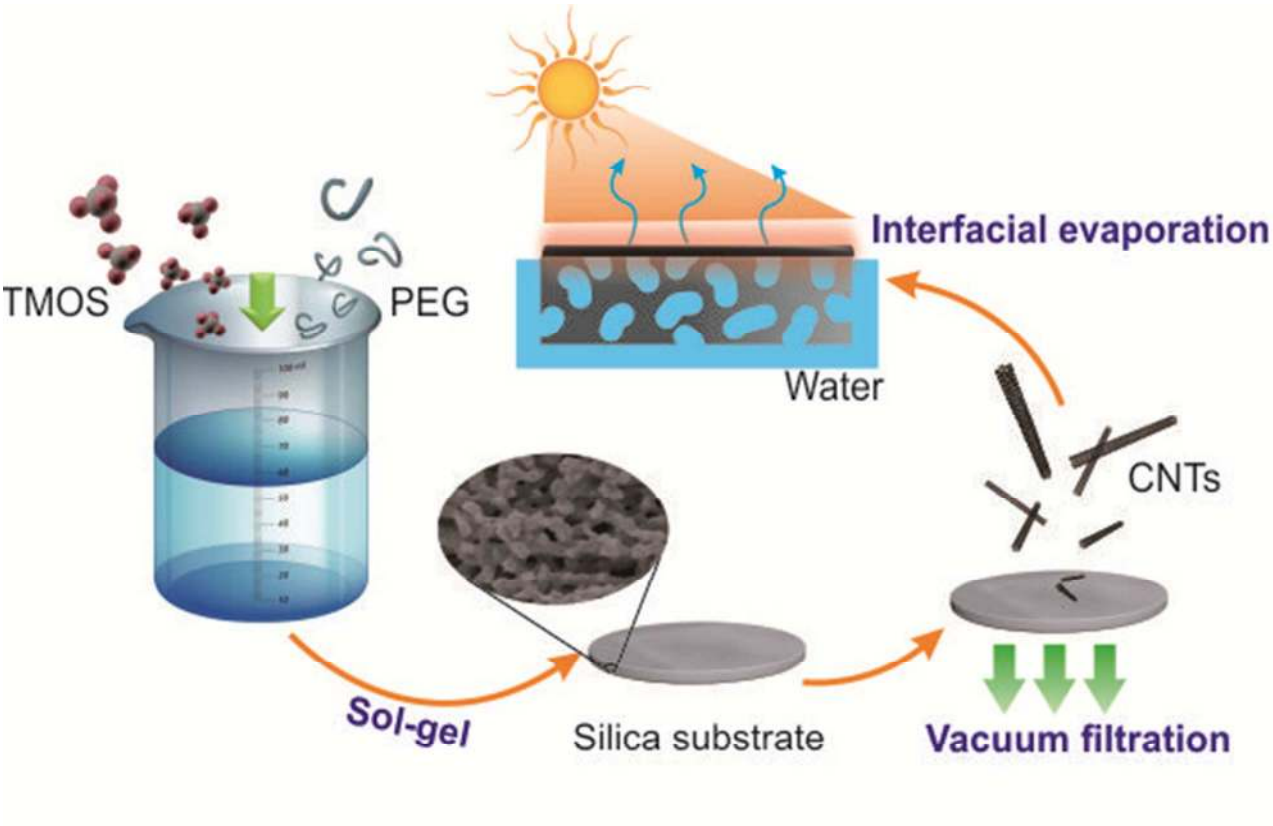

Figure 1. Schematic illustration of preparation of the CNT-silica bi-layered material. The macroporous silica substrate was prepared *via* sol-gel process. CNT membrane was coated on top of the silica substrate by vacuum filtration. The bi-layered material self-floated at the air-water interface, captured solar light and converted it to heat for water evaporation.

Figure 1 presents a schematic of the material preparation. Briefly, the macroporous silica sheet was fabricated by using TMOS as silica source and PEG as the pore formation agent *via* sol-gel

process.(27) The shape and size of the silica sheet can be easily controlled by the shape and size of the container. SEM images revealed that the synthesized silica substrate had interconnected worm-like macroporous structure, and the pore size was around 2.2 μm (Figure S1), which agrees well with the pore size measured by mercury porosimetry (Figure S2). This pore size, according to the literature reports and the results of this project, is large enough for efficient water pumping (Figure S3). The bulk density of the macroporous silica substrate was as low as 0.2 g cm^{-3}, indicating the porosity of this material was as high as 90 %. A surfactant stabilized CNT dispersion was then vacuum filtrated onto the macroporous silica sheet to form a top CNT membrane.

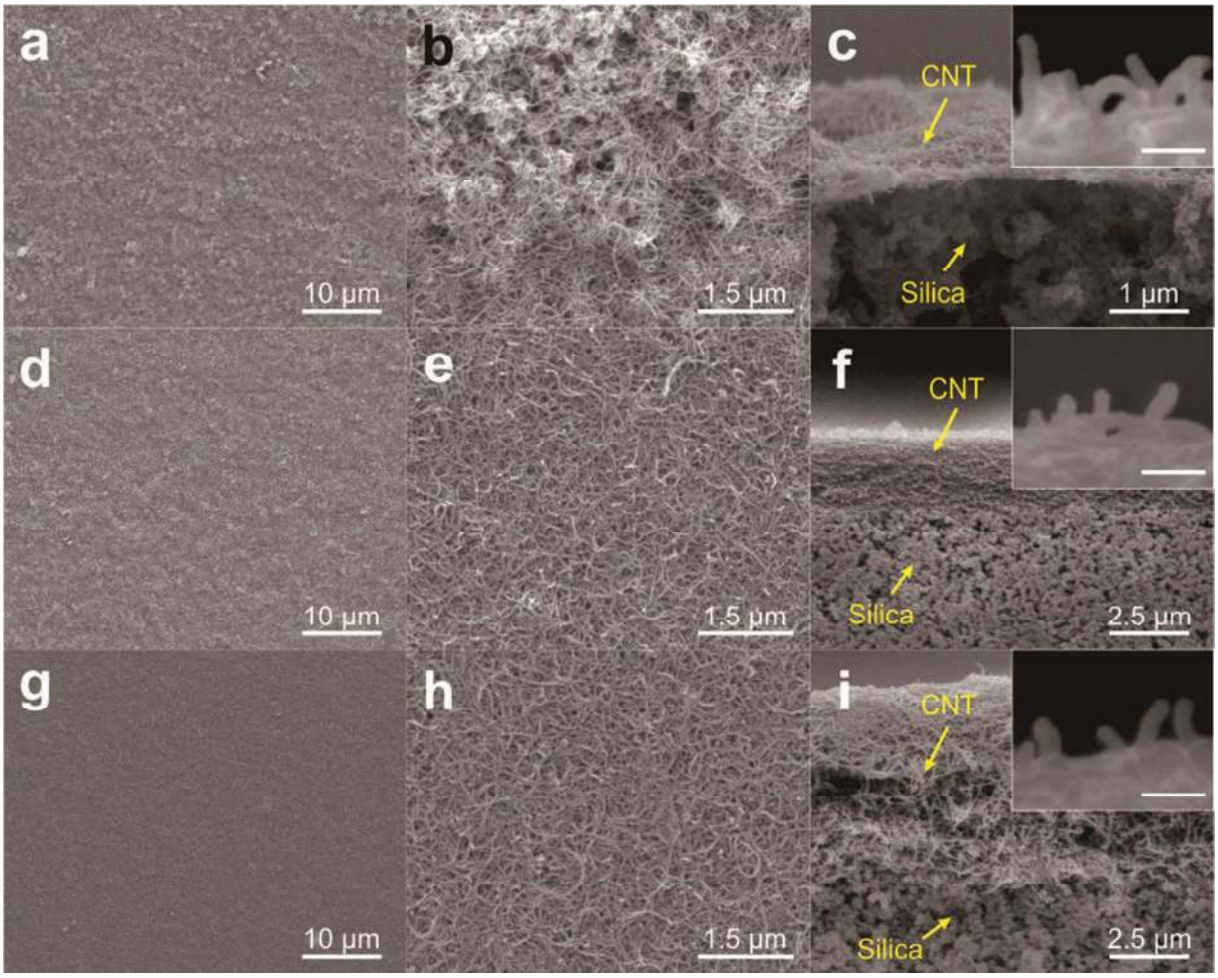

Figure 2. SEM images of the CNT-silica bi-layered material with CNT layer thickness of (a-c) 0.1 μm, (d-f) 2.4 μm and (g-i) 5.6 μm, on top of the macroporous silica substrate with thickness at 0.3 mm. Inset images in c, f, and i have scale bars at 100 nm and show there were some upright CNTs on the surfaces.

The diameter of the CNTs was approximately 13 nm, which is much smaller than the pore size of the silica substrate, and the length of the CNTs was generally greater than 5 μm, exhibiting a large length-diameter ratio (Figure S4). At the end of the vacuum filtration, formed on top of the silica substrate was a CNT film layer whose thickness could be adjusted by varying the volume of the initial CNT dispersion (Figure S5). Figures 2 and S6 present the SEM images of the porous CNT layers with thickness from 0.1 to 5.6 μm sitting on top of the macroporous silica substrate. As can be observed, the surface roughness of the CNT layers decreased with their thickness (Figures 2b, 2e and 2h). Interestingly, the cross-section view SEM images revealed that there was abundant somewhat upright nanotubes on the CNT layer surfaces (Figure 2c, f, i) in all cases. This kind of CNT surface structure is advantageous as it has been reported that vertically aligned CNT array can greatly decrease the light reflection and thus increase the solar energy harvest efficiency.(16-17) In case of the CNT layer with 0.1 μm thickness (Figures 2a-c), its surface was not uniformly covered by the CNTs and some silica substrate domains could be visible from top (Figure 2b), while for the thickness of 2.4 and 5.6 μm, uniform CNT surfaces were obtained.

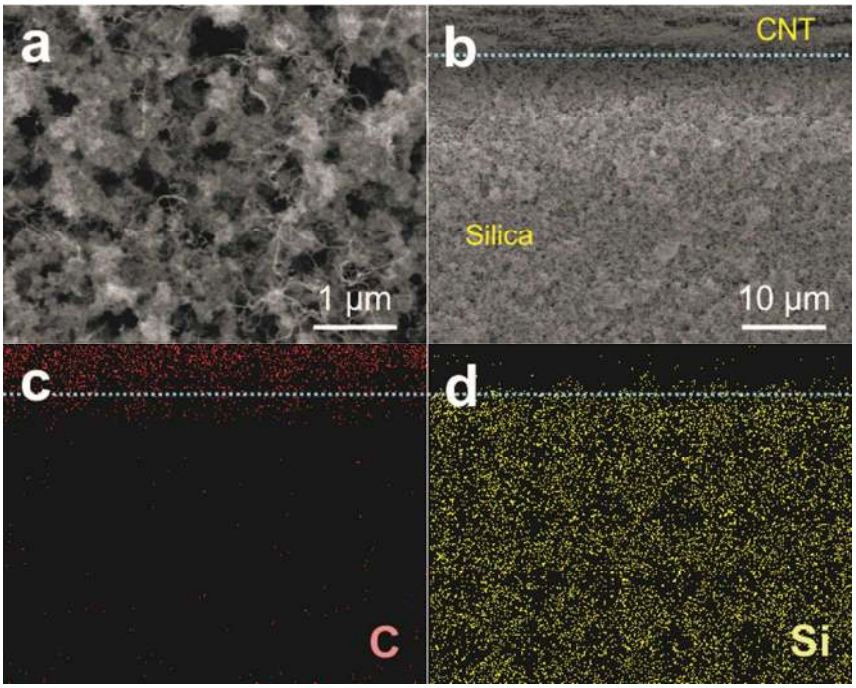

Figure 3. (a) SEM image of the silica substrate after removing the top CNT layer. Some CNTs were found infiltrated into the macropores of the silica substrate. (b) SEM image of the cross section view of the bi-layered material, consisting of a 5.6 μm thick CNT layer on top of a 0.3 mm thick silica substrates and the corresponding elemental mapping images of (c) carbon and (d) silicon from the EDS analyses. The dashed lines in (b-d) are the physical boundary between the CNT and silica substrate.

Figure 3a shows a top view of a CNT-silica bi-layered material after removing the CNT membrane layer, which clearly reveals that some carbon nanotubes infiltrated into the macropores of the top portion of the silica substrate (Figure S7) and agrees well with the cross-section SEM image (Figure 3b). This feature is beneficial for seamless connection of the two layers and ensures two layers not to detach from each other once in water. In contrast, the CNT membrane formed on a hydrophilic glass slide or silicon wafer tended to separate from the substrate once in contact with water (Figure S8). The elemental mapping results also confirm

that the infiltration of the CNTs was restrained only within the small top portion of the silica substrate (Figure 3c and 3d). As a control experiment, a self-supporting CNT membrane without the underlying silica substrate was similarly prepared on a silicon wafer and showed a smoother surface without upright nanotubes on its surface (Figure S9-10). This leads us to believe that the infiltration of the CNTs into the macropores of the silica substrate contributed to the formation of its rough CNT surface with upright surface structure, which is an attractive feature in light adsorption. The bulk density of the CNT membrane formed on the macroporous silica substrate surface was 0.4 g cm^{-3} with a porosity of 80 %, indicating its highly porous structure.

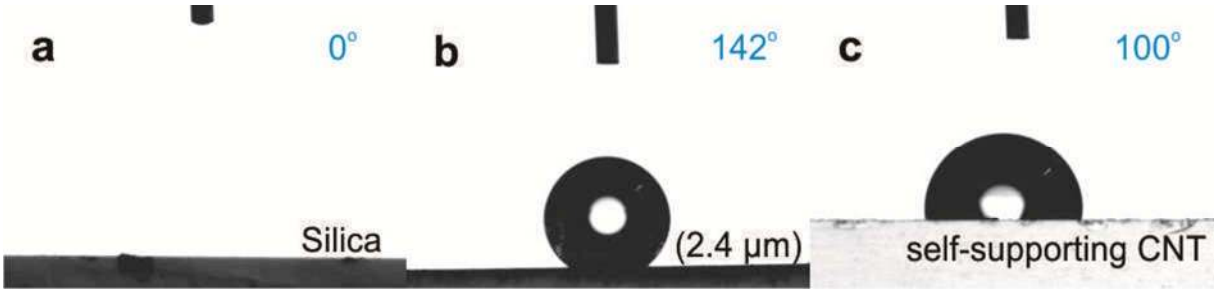

Figure 4. Water contact angles of (a) macroporous silica substrate, (b) CNT-silica bi-layered material with CNT layer thickness of 2.4 μm and (c) self-supporting CNT membrane.

The water contact angle of the pristine macroporous silica substrate was 0°, indicating its superhydrophilicity (Figure 4a). The water contact angles of the CNT membranes in the bi-layered samples before and after the surfactant removal were 0° and 142° respectively (Figure 4b and S11a), indicating the critical role of surfactant removal (Figure S12). The hydrophobicity of the CNT layer after the surfactant removal gave rise to self-floating capability in water to the bi-layered composite materials (Figure S11b). In comparison, the water contact angle of the self-supporting CNT membrane prepared on a silicon wafer was lower (i.e., 100°) (Figure 4c), presumably due to its relatively smooth surface than the CNT membrane prepared on top of the porous silica substrate.

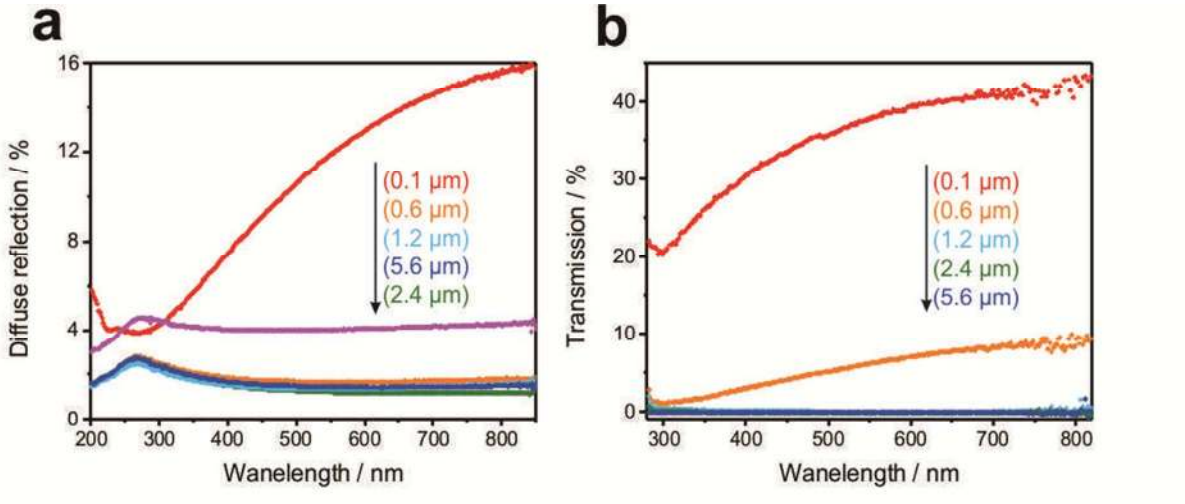

Figure 5. (a) The diffuse reflection and (b) transmission spectra of the CNT top layers separated from the CNT-silica bi-layered materials.

Figure 5 shows the light diffuse reflection and transmission of the CNT top layers within UV and visible range (200 to 800 nm). Among the samples tested, the ones with thickness from 1.2 μm to 2.4 μm exhibited average diffuse reflection less than 2 % and almost zero transmission, indicating nearly full light harvesting. The low light reflection by the CNT top layers can be attributed to the great light adsorption of carbon-based material as well as the upright surface nanotube structure. In comparison, the self-supporting CNT membrane prepared on the silicon wafer showed a diffuse reflection over 4 % (Figure S13), implying the special upright nanotube surface structure is beneficial for light harvesting.

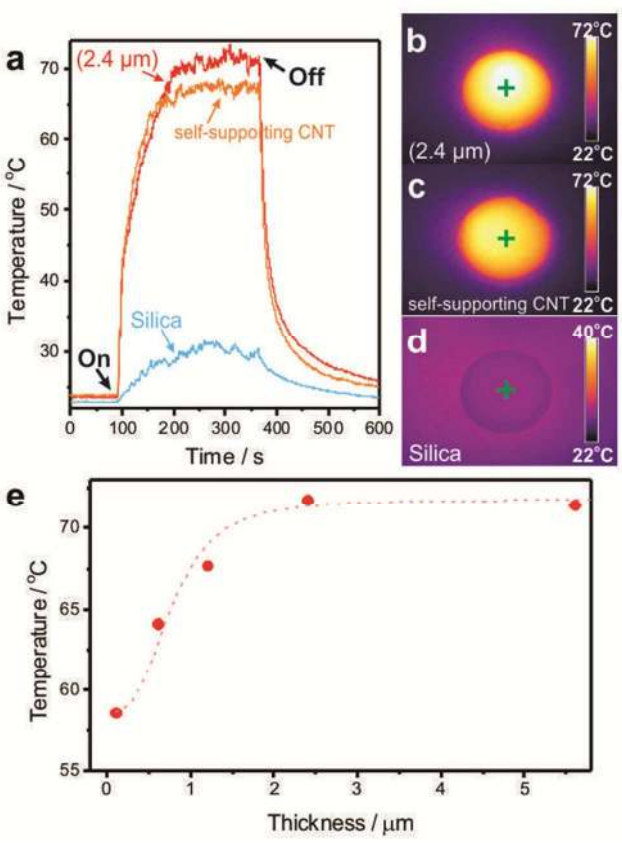

Figure 6. (a) Time-course of the temperature curves in response to light illumination and the IR thermal images of (b) the bi-layered material with CNT layer thickness of 2.4 μm, (c) self-supporting CNT membrane, and (d) 0.3 mm thick silica substrate without CNT membrane, under the simulated solar light irradiation for 300 s in air at room temperature. The markers (+) in the thermal images show the spots where temperature curves were recorded. The diameters of samples in (b-d) were all 2.5 cm. Signs of 'on' and 'off' in (a) indicate the time when the solar light was switched on and off. (e) The equilibrium temperatures of the CNT-silica bi-layered materials in air under the simulated solar irradiation.

Figures 6a-d compare the surface temperatures of three different samples in air under light illumination. The temperature data and images were captured by the infrared camera. In taking the temperature measurement, all of the tested samples were placed on a polystyrene foam plate

to minimize the heat exchange with the underlying base. In the absence of the CNT top layer, the macroporous silica substrate showed only a slow and small temperature rise and achieved an equilibrium temperature of 31 °C under the irradiation due to the poor light harvest efficiency. In contrast, upon the light illumination, the temperature of the CNT-silica bi-layered material rose sharply to an equilibrium temperature at around 72 °C, indicating good photothermal performance of the CNT layer, which is attributed to the great solar light absorbance and low specific heat capacity of the CNTs. The self-supporting CNT membrane showed a similar temperature rising limb, but with a slightly lower equilibrium temperature of 68 °C. Figure 6e presents the equilibrium surface temperatures of the CNT-silica bi-layered materials as a function of CNT layer thickness. As can be seen, the equilibrium temperature increased with the thickness of the CNT layer before reaching a plateau temperature at 72 °C at the thickness of 2.4 μm. The above results demonstrate that the highly efficient light harvesting and light-to-heat conversion of the CNT top layer when its thickness ≥ 2.4 μm.

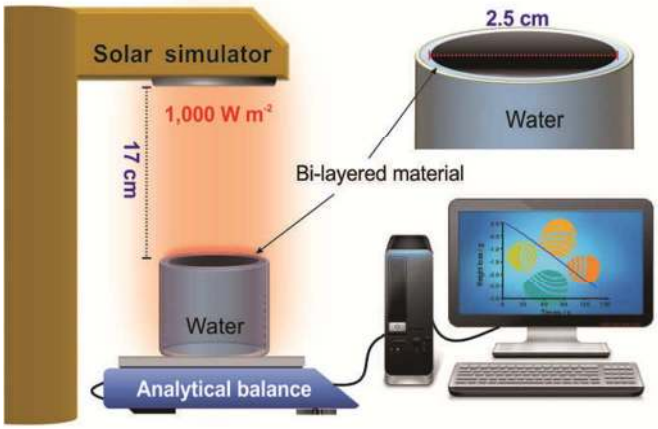

Scheme 1. Schematic illustration for the setup of the water evaporation measurement with the CNT-silica bi-layered material floating on the water surface. Inset image shows the bi-layered material floating on the water surface in the PP cup.

The water evaporation performance of the CNT-silica bi-layered materials was then systematically investigated by using a lab-made on-line, real-time measurement system (Scheme 1). With the CNT-silica bi-layered material with CNT layer thickness of 2.4 μm floating on top of water, the water evaporation rate under illumination was 3 times that without the bi-layered material (1.25 vs. 0.40 kg m^{-2} h^{-1}) (Figure 7a), which is attributed to the interfacial heating scheme in the former through exclusively localized solar energy harvesting and highly efficient heat generation by the composite material. The water evaporation rate increased gradually in the first 30 min before reaching a stable level (Figure 7b). Figure 7c presents water evaporation rates as a function of the thickness of the CNT top layers. The water evaporation rate increased with the CNT layer thickness, with the 0.1 μm thick CNT layer performing the worst at 0.75 kg m^{-2} h^{-1} and 2.4 μm and 5.6 μm of CNT layers performing comparably. This result agrees well with the light adsorption and heat generation performances of these materials (Figure 5 and Figure 6e).

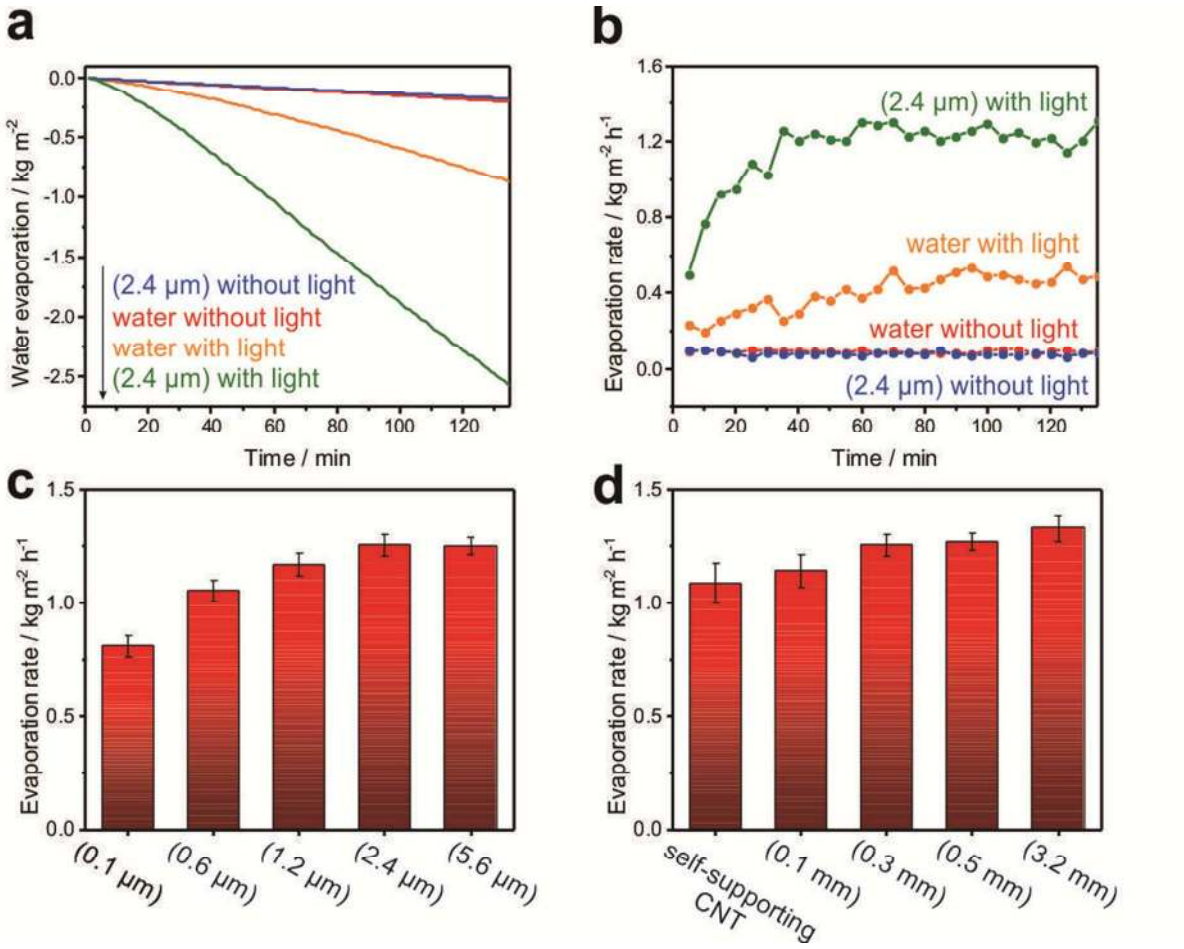

Figure 7. (a) Time-course of water evaporation performance under various conditions and (b) corresponding average water evaporation rates. The average water evaporation rates of the bi-layered samples with (c) different CNT layer thickness on 0.3 mm thick silica substrate, and (d) different silica substrate thickness with a constant CNT layer thickness at 2.4 μm and a self-supporting CNT membrane with a thickness of 7.1 μm after 30 min illumination.

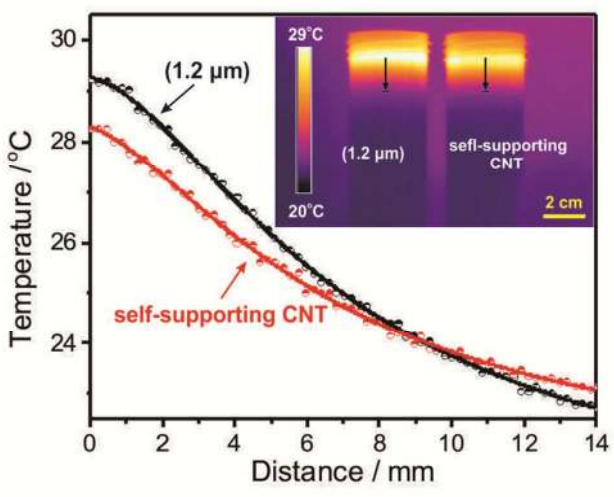

Figure 8. The temperature profile comparison in the presence of the bi-layered materials with 0.3 mm thick silica substrate *versus* self-supporting CNT membrane under light irradiation on for 30 min. The thickness of CNT layer of the bi-layered material was 1.2 μm. Inset is the IR thermal images. The distance is defined as downward distance from the central location of the top CNT layer in water.

In addition, the effect of the thickness of the macroporous silica substrate was also investigated. The water evaporation performance of a series of the bi-layered samples with same CNT layer thickness (2.4 μm) but different macroporous silica thickness were examined and is presented in Figure 7d. The self-supporting CNT membrane was also included as a control sample, who obtained an average water evaporation rate of 1.09 kg m^{-2} h^{-1}. The water evaporation rate was increased to 1.25, 1.27 and 1.31 kg m^{-2} h^{-1}, with the thickness of the silica substrate at 0.3, 0.5 and 3.2 mm, respectively, indicating the beneficial role of the silica substrate. It was difficult to keep the bi-layered materials floating on water surface when the thickness of the silica substrate was larger than 3.2 mm.

Figure 8 shows the temperature profile of in the presence of CNT-silica bi-layer sample *versus* self-supporting CNT membrane on top of water. The bi-layered material with 1.2 μm thick CNT

layer was chosen in the experiment because the surface temperature was similar to the self-supporting CNT membrane under illumination in air. As can be seen, with the CNT-silica bi-layered material floating on top of water, a shaper temperature gradient was created in the system than that with the self-supporting CNT membrane due to the heat barrier role of the silica substrate. The sharper temperature gradient translates directly to higher extent of heat confinement within the top interfacial water region and less heat dissipation to the non-evaporative portion of the bulk water. The heat confinement could be further promoted with increasing silica substrate thickness (Figure S15).

It has been reported that a hydrophilic porous substrate with suitable pore size can pump water up to the air-water interface due to the capillary effect.(11) To prove the water pumping effect of the silica substrate, a bi-layered CNT-silica sample was prepared by coating a CNT membrane on a silica monolith with a conical bottom, which was then placed on a glass vial filled with water as shown in Figure S16a-b. The seams between the tube and sample were sealed off with vaseline. This size of the silica substrate cone and the glass vial mouth was such that the water inside the vial couldn't contact with the CNT layer directly and the water could only be pulled up through the macroporous channels inside the silica substrate. The setup was then exposed to simulated solar light and a high and constant water evaporation rate of 1.25 kg m^{-2} h^{-1} was obtained (Figure S16c). This result demonstrates that the hydrophilic silica support had the capability of pumping water from the underlying bulk water to the air-water interface. Therefore, the macroporous silica substrate is an essential component of the bi-layered material in obtaining a high and sustained water evaporation rate.

The solar thermal conversion efficiency (η), which is defined in equation (3), is considered as an important index to evaluate the performance:

$$\eta = \frac{H_e}{Q_s} \times \frac{dm}{dt} = \frac{H_e \times v}{Q_s} \quad (3)$$

where Q_s is the incidence light power (1,000 W m^{-2}), m is the mass of evaporated water, t is time, v is the evaporation rate of water, and H_e is the heat of evaporation of water (2260 kJ kg^{-1}). According to the equation (3), the solar thermal conversion efficiency of the CNT-silica bi-layered material could reach up to 82%, with the evaporation rate at 1.31 kg m^{-2} h^{-1}. The water evaporation performance of the CNT-silica bi-layered materials compare favorably against other materials in the literature. (8-11)

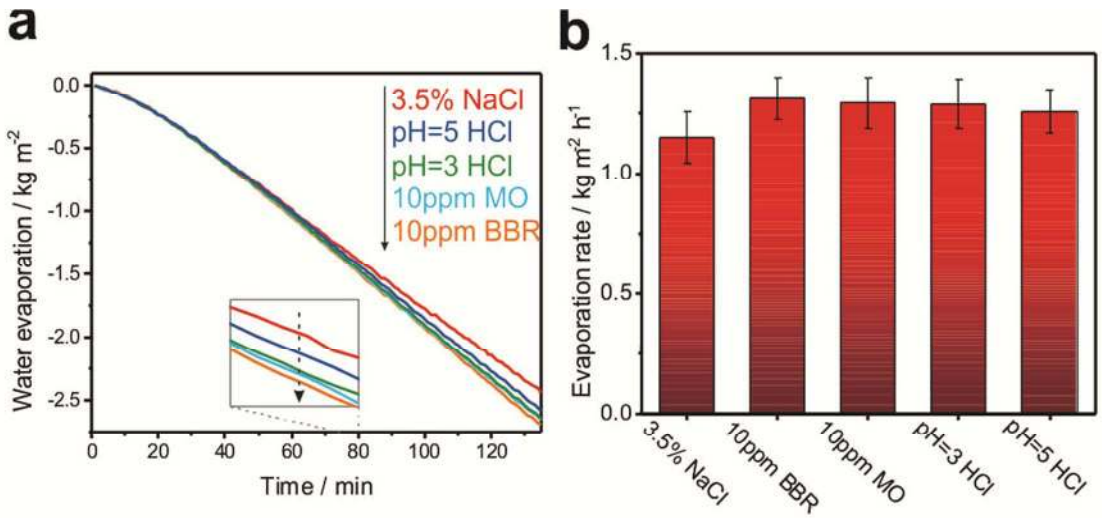

Figure 9. (a) Time-course of water evaporation from different water and (b) corresponding average evaporation rates after 30 min illumination.

The solar-driven water evaporation performance of the bi-layered material with CNT layer thickness of 2.4 μm and 0.3 mm thick silica substrate was further evaluated under environmentally relevant water conditions, including 3.5 wt % NaCl solution, 10 ppm brilliant blue R (BBR) aqueous solution, 100 ppm methyl orange (MO) aqueous solution, and HCl aqueous solutions with pH=3 and pH=5. The corresponding water evaporation rates are presented in Figure 9 and are within the range of 1.15 to 1.29 kg m^{-2} h^{-1}. The solar thermal

conversion efficiencies were in the range between 72-81%. These results demonstrate the versatility of the bi-layered materials in terms of their applicable water conditions.

CONCLUSION

In summary, we have designed and fabricated the CNT-silica bi-layered material for highly efficient solar-driven water evaporation. The CNT layer acted as extraordinary photothermal material with high absorbance in solar light and the macroporous silica substrate was essential in forming desirable surface CNT micro-structures and performing as a heat barrier. The two rationally designed layers worked synergistically in obtaining highly efficient solar-to-heat conversion for water evaporation. We believe that the rationally designed material has a great potential to be used in the wide field of photothermal-based water applications, such as water distillation and water desalination, especially in point-of-use front.

ASSOCIATED CONTENT

Supporting Information. This material is available free of charge via the Internet at http://pubs.acs.org. The Supporting Information includes SEM and TEM images of the CNTs, macroporous silica substrate; water wettability of the materials; average thickness of the CNT layer as a function of the volume of the initial CNT dispersion; FTIR spectra of the bi-layered material before and after washed; the reflection of the self-supporting CNT membrane; the temperature profile of the water in the presence of the bi-layered materials with different silica thickness under light irradiation; Time-course of water evaporation performance of the bi-layered material with cone-shaped silica substrate.

AUTHOR INFORMATION

Corresponding Author

*Peng Wang. E-mail: peng.wang@kaust.edu.sa.

Notes

The authors declare no competing financial interest

ACKNOWLEDGMENT

The authors are grateful to the teammates of the KAUST Environmental Nanotechnology Laboratory for very helpful scientific discussions. The project was funded by KAUST CRG-3.

REFERENCES

1. Chu, S.; Majumdar, A., Opportunities and challenges for a sustainable energy future. *Nature* **2012,** *488* (7411), 294-303.
2. Lewis, N. S.; Nocera, D. G., Powering the planet: Chemical challenges in solar energy utilization. *Proceedings of the National Academy of Sciences* **2006,** *103* (43), 15729-15735.
3. Calvin, M., Solar-Energy by Photosynthesis. *Science* **1974,** *184* (4134), 375-381.
4. Kamat, P. V., Meeting the clean energy demand: Nanostructure architectures for solar energy conversion. *J Phys Chem C* **2007,** *111* (7), 2834-2860.
5. Zhang, L.; Tang, B.; Wu, J.; Li, R.; Wang, P., Hydrophobic Light-to-Heat Conversion Membranes with Self-Healing Ability for Interfacial Solar Heating. *Advanced Materials* **2015,** *27* (33), 4889-4894.
6. Wang, Z.; Liu, Y.; Tao, P.; Shen, Q.; Yi, N.; Zhang, F.; Liu, Q.; Song, C.; Zhang, D.; Shang, W.; Deng, T., Bio-Inspired Evaporation Through Plasmonic Film of Nanoparticles at the Air–Water Interface. *Small* **2014,** *10* (16), 3234-3239.
7. Li, R.; Zhang, L.; Wang, P., Rational design of nanomaterials for water treatment. *Nanoscale* **2015,** *7* (41), 17167-17194.
8. Yu, S.; Zhang, Y.; Duan, H.; Liu, Y.; Quan, X.; Tao, P.; Shang, W.; Wu, J.; Song, C.; Deng, T., The impact of surface chemistry on the performance of localized solar-driven evaporation system. *Scientific Reports* **2015,** *5*, 13600.
9. Ghasemi, H.; Ni, G.; Marconnet, A. M.; Loomis, J.; Yerci, S.; Miljkovic, N.; Chen, G., Solar steam generation by heat localization. *Nat Commun* **2014,** *5*.

10. Liu, Y.; Yu, S.; Feng, R.; Bernard, A.; Liu, Y.; Zhang, Y.; Duan, H.; Shang, W.; Tao, P.; Song, C.; Deng, T., A Bioinspired, Reusable, Paper-Based System for High-Performance Large-Scale Evaporation. *Advanced Materials* **2015,** *27* (17), 2768-2774.
11. Ito, Y.; Tanabe, Y.; Han, J.; Fujita, T.; Tanigaki, K.; Chen, M., Multifunctional Porous Graphene for High-Efficiency Steam Generation by Heat Localization. *Advanced Materials* **2015,** *27* (29), 4302-4307.
12. Neumann, O.; Urban, A. S.; Day, J.; Lal, S.; Nordlander, P.; Halas, N. J., Solar Vapor Generation Enabled by Nanoparticles. *ACS Nano* **2013,** *7* (1), 42-49.
13. Zeng, Y.; Wang, K.; Yao, J.; Wang, H., Hollow carbon beads for significant water evaporation enhancement. *Chemical Engineering Science* **2014,** *116*, 704-709.
14. Zeng, Y.; Yao, J.; Horri, B. A.; Wang, K.; Wu, Y.; Li, D.; Wang, H., Solar evaporation enhancement using floating light-absorbing magnetic particles. *Energy & Environmental Science* **2011,** *4* (10), 4074-4078.
15. Liu, Y.; Chen, J.; Guo, D.; Cao, M.; Jiang, L., Floatable, Self-Cleaning, and Carbon-Black-Based Superhydrophobic Gauze for the Solar Evaporation Enhancement at the Air–Water Interface. *ACS Applied Materials & Interfaces* **2015,** *7* (24), 13645-13652.
16. Yang, Z.-P.; Ci, L.; Bur, J. A.; Lin, S.-Y.; Ajayan, P. M., Experimental Observation of an Extremely Dark Material Made By a Low-Density Nanotube Array. *Nano Letters* **2008,** *8* (2), 446-451.
17. Panagiotopoulos, N. T.; Diamanti, E. K.; Koutsokeras, L. E.; Baikousi, M.; Kordatos, E.; Matikas, T. E.; Gournis, D.; Patsalas, P., Nanocomposite Catalysts Producing Durable, Super-Black Carbon Nanotube Systems: Applications in Solar Thermal Harvesting. *ACS Nano* **2012,** *6* (12), 10475-10485.
18. Bartlett, D. F., Physics for Scientists and Engineers with Modern Physics - Serway,Ra. *Phys Teach* **1984,** *22* (7), 468-&.
19. Cao, A.; Zhang, X.; Xu, C.; Wei, B.; Wu, D., Tandem structure of aligned carbon nanotubes on Au and its solar thermal absorption. *Solar Energy Materials and Solar Cells* **2002,** *70* (4), 481-486.
20. Kolpak, A. M.; Grossman, J. C., Azobenzene-Functionalized Carbon Nanotubes As High-Energy Density Solar Thermal Fuels. *Nano Letters* **2011,** *11* (8), 3156-3162.
21. Shannon, M. A.; Bohn, P. W.; Elimelech, M.; Georgiadis, J. G.; Marinas, B. J.; Mayes, A. M., Science and technology for water purification in the coming decades. *Nature* **2008,** *452* (7185), 301-310.
22. Pendergast, M. M.; Hoek, E. M. V., A review of water treatment membrane nanotechnologies. *Energy & Environmental Science* **2011,** *4* (6), 1946-1971.
23. Wu, Z.; Chen, Z.; Du, X.; Logan, J. M.; Sippel, J.; Nikolou, M.; Kamaras, K.; Reynolds, J. R.; Tanner, D. B.; Hebard, A. F.; Rinzler, A. G., Transparent, Conductive Carbon Nanotube Films. *Science* **2004,** *305* (5688), 1273-1276.
24. Wen, D.; Ding, Y., Effective Thermal Conductivity of Aqueous Suspensions of Carbon Nanotubes (Carbon Nanotube Nanofluids). *Journal of Thermophysics and Heat Transfer* **2004,** *18* (4), 481-485.
25. Pradhan, N. R.; Duan, H.; Liang, J.; Iannacchione, G. S., The specific heat and effective thermal conductivity of composites containing single-wall and multi-wall carbon nanotubes. *Nanotechnology* **2009,** *20* (24).
26. Yi, W.; Lu, L.; Zhang, D. L.; Pan, Z. W.; Xie, S. S., Linear specific heat of carbon nanotubes. *Phys Rev B* **1999,** *59* (14), R9015-R9018.

27. Tao, S. Y.; Wang, Y. C.; An, Y. L., Superwetting monolithic SiO2 with hierarchical structure for oil removal. *Journal of Materials Chemistry* **2011,** *21* (32), 11901-11907.

Self-floating carbon nanotube membrane on macroporous silica substrate for highly efficient solar-driven interfacial water evaporation

*Yuchao Wang, Lianbin Zhang, and Peng Wang**

Water Desalination and Reuse Center, Division of Biological and Environmental Science and Engineering, King Abdullah University of Science and Technology, Thuwal 23955-6900, Saudi Arabia.

*Corresponding author: Peng Wang, e-mail: peng.wang@kaust.edu.sa.

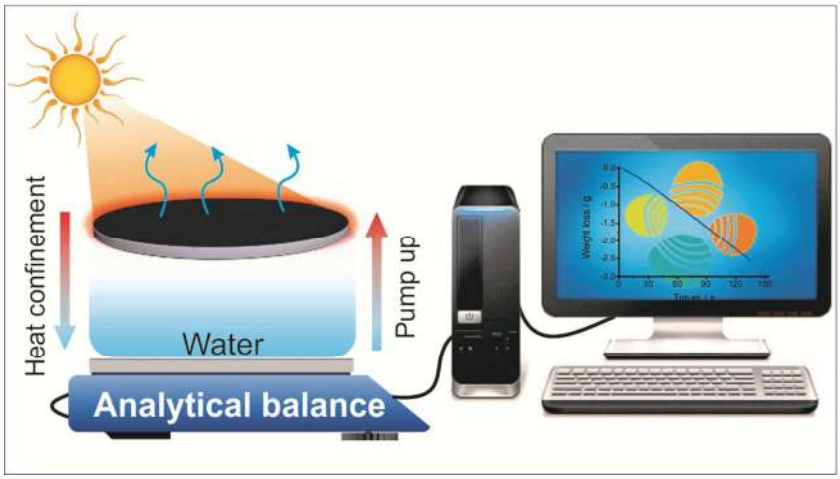

A bi-layered material based on CNT membrane and silica support was rationally designed and fabricated for solar-driven water evaporation for portable water production.